Implementation of a finite element model for gear stress analysis based on tie-surface constraints and its validation through the Hertz's theory

Ignacio Gonzalez-Perez*

Department of Mechanical Engineering
Politechnic University of Cartagena
Cartagena, Spain, 30202
Email: ignacio.gonzalez@upct.es

Alfonso Fuentes-Aznar

Department of Mechanical Engineering
Rochester Institute of Technology
Rochester, NY, USA
Email: afeme@rit.edu

ABSTRACT

A new finite element model for stress analysis of gear drives is proposed. Tie-surface constraints are applied at each tooth of the gear model to obtain meshes that can be independently defined: a finer mesh at contact surfaces and fillet and a coarser mesh in the remaining part of the tooth. Tie-surface constraints are also applied for the connection of several teeth in the model. The model is validated by application of the Hertz's theory in a spiral bevel gear drive with localized bearing contact and by observation of convergency of contact and bending stresses. Maximum contact pressure, maximum Mises stress, maximum Tresca stress, maximum major principal stress, and loaded transmission errors are evaluated along two cycles of meshing. The effects of the boundary conditions that models with three, five, seven, and all the teeth of the gear drive, provide on the above mentioned variables are discussed. Several numerical examples are presented.

1 Introduction

Application of the finite element method for stress analysis in gear drives is a common practice in many specific sectors (automobile, naval, aeronautic, and so on). The maximum contact pressure on the contacting surfaces, or the maximum Von Mises stress underneath the contacting surfaces, are needed to evaluate the capability of the to-be-manufactured gear drive. Accurate results require models with a fine mesh in the contact region where the contact occurs, and in the fillet region where bending stresses are higher, whereas a coarse mesh can be applied to other parts of the gear body, far from the areas of interest, as long as the model keeps its capability to represent tooth bending, gear torsion, wedge bending, and so on.

Different finite element models have been proposed since the first application of the finite element method to the investigation of stresses in gear drives [1, 2]. A step forward in the development of a finite element model for stress analysis of gear drives was presented in [3], allowing the analysis of the whole cycle of meshing through the application of a given torque to the pinion member whereas the gear is rotated and held at rest at each contact position. Rigid boundary conditions on the rims were considered, far enough from the contact areas to avoid any interference with the sought-for stresses. Later, a finite element model to consider the effect of the torsional deformation of the gear bodies in the formation of the bearing contact was implemented [4]. Investigation of wedge bending and rim thickness in contact and bending stresses was presented in [5, 6]. The effect of shaft deflections in the formation of the bearing contact was considered later in [7] and as a method to determine machine-tool settings corrections in [8].

*Corresponding author, phone: +34968326429, fax: +34968326449.

Along the history of development of finite element models for gears, some efforts have been directed towards the reduction of the computational cost, one of the main drawbacks of this approach. Application of multi-point constraints for a rapid transition through the mesh of the gear tooth was applied in [9] for a two-dimension problem and in [10] for a three-dimension problem. Multi-point constraints allows a transition from two or four elements to one element by constraining some degrees of freedom. A finite element model based on tie-surface constraints was presented in [11] for a transmission with three spur gears in order to consider two parts in the gear body, one with a fine mesh close to the area of interest, and the other one with a coarse mesh. Some other efforts have been focused on combining finite element models with semi-analytical approaches [12]. All these efforts for the reduction of the computational cost are important in the optimization process of gear drives to get competitive transmissions [13, 14].

Some questions still arise among users of the finite element method in gear design:

(1) Capability of a given model to capture the evolution of the maximum Von Mises or Tresca stress underneath the contacting surfaces. This issue is important, not only to know the maximum stress that represents the root cause for pitting, but also to know the depth at which this stress occurs since it will affect to the selection and configuration of the hardening process.
(2) Capability of a given model to capture the evolution of the maximum contact pressure. Such a pressure can be compared with the contact strength of gear materials which are based on tests.
(3) Capability of a given model to capture the evolution of maximum major principal stress in the fillet region. Here, some other questions arise as how far the boundary conditions have to be from the contact area to obtain reliable results, or if the gear tooth or the gear body are appropriately modeled.
(4) Application of linear elements versus quadratic elements in the contact region.

The main goal of this paper is to find answers to the above mentioned issues for which the following objectives have been proposed:

(i) Implementation of a finite element model for any type of gear drive based on tie-surface constraints. Some of these constraints allow each gear tooth to be divided into two parts. One of these parts is closer to the contact and fillet regions for the development of a finer mesh. A coarse mesh is applied in the other part of the gear model to reduce the computational cost. Some other tie-surface constraints are applied to connect different teeth in the model.
(ii) Application of the Hertz's theory to validate the proposed finite element model in terms of maximum contact pressure, maximum Von Mises stress and maximum Tresca stress. Application of the Hertz's theory is important here to determine the appropriate thickness of the finer-mesh part and the depth at which these maximum stresses are reached.
(iii) Investigation of the effects of proximity of the boundary conditions on bending and contact stresses and on the function of loaded transmission errors through consideration of models with one, three, five, and seven pairs of teeth. The possibility of using a whole gear drive model is also presented and compared with the previous models.

Application of the Hertz's theory to analyze contact stresses in gear drives has several limitations. A hertzian contact requires a gap between the contacting surfaces that can be modeled through a function of type $h(x,y) = c_x x^2 + c_y y^2$. Here, the gap h can be stated as a function of two independent variables x and y with coefficients c_x and c_y that depend on the relative curvatures of pinion and gear tooth surfaces [15]. This is the main reason why a spiral bevel gear drive with double crowned tooth surfaces is considered here. Contact stresses provided by the proposed model are compared to Hertz stresses. The Hertz's theory has been applied in the analysis of spur gear drives in [16, 17]. The same ideas are extended here for the case of a spiral bevel gear drive as it will be shown in the numerical example. Although the implemented finite element model is applied to a spiral bevel gear drive, the same ideas can be easily extended to other types of gear drives.

2 Development of the finite element model

The finite element model has, for each tooth, two different parts that are meshed independently, the contact-fillet region for a finer mesh, and the tooth body region for a coarse mesh (see Figs. 1 and 2). Such meshes are generated automatically as a function of the point coordinates that are determined from application of gear theory and following the prescribed generating motions of each gear and its corresponding tool [18]. The finite element model is developed through the following stages:

(1) Determination of point coordinates on the gear tooth surfaces for the definition of the tooth body mesh (see Fig. 1(a)). The point coordinates are determined from application of gear theory as a function of the number of elements in longitudinal, profile, and fillet directions. Quadratic elements are considered here in order to capture the longitudinal curvature of the gear (as in helical, spiral bevel or hypoid gears) with few elements along longitudinal direction. A reduced number of finite elements is considered in the profile and in the fillet directions (4 elements in profile direction and 2 elements in the fillet direction). The obtained points are used as a reference to define the designed volume to be meshed.
(2) The designed volume is divided considering auxiliary surfaces from (1) to (6) and an intermediate surface S as it is illustrated in Fig. 1(b). These surfaces are obtained from intermediate points, which are derived from the point coordinates

mentioned above. Intermediate surface S separates the tooth body region from the contact-fillet region and is defined parallel to the contact and fillet tooth surfaces by an amount equal to $c_t m_{ot}$. Here, c_t is a coefficient and m_{ot} is the module (the outer transverse module for a spiral or an hypoid type) of the gear drive.

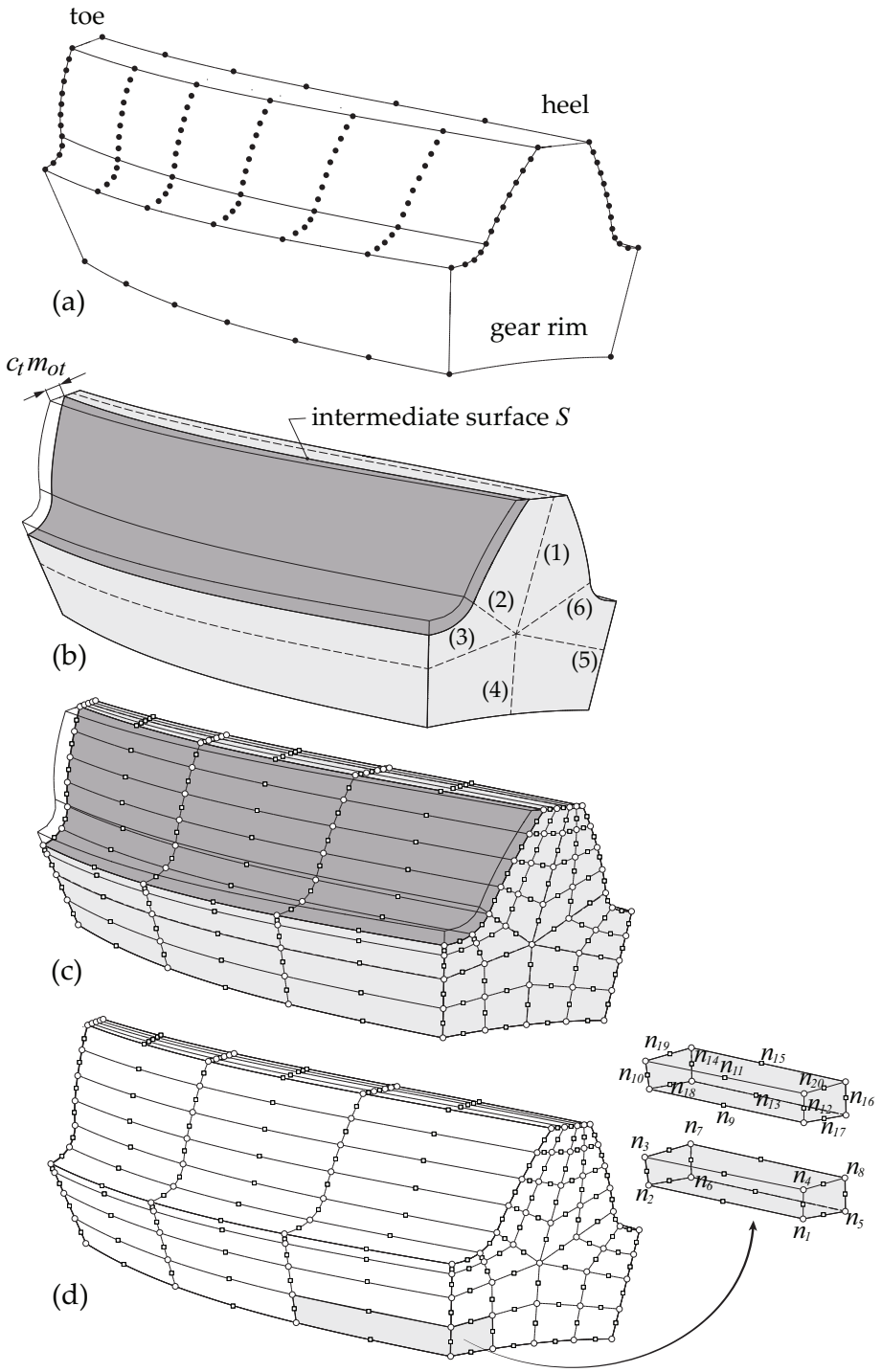

Fig. 1. For mesh definition of tooth body region: (a) designed volume with obtained points from application of gear theory, (b) auxiliary surfaces and intermediate surface S, (c) nodes, and (d) finite elements.

(3) Node coordinates are determined in the tooth body region from the obtained point coordinates considering the auxiliary surfaces and the intermediate surface S (see Fig. 1(c)). Not all the point coordinates are used for the determination of the nodes since quadratic elements are considered here.
(4) Finite elements are built from the obtained nodes following the numbering for node connectivity shown in Fig. 1(d).

(5) New point coordinates are determined on the gear tooth surfaces for the definition of the contact-fillet region mesh and as a function of the number of elements in longitudinal, profile and fillet directions (see Fig. 2(a)). A number of layers of elements is also defined (3 layers of elements are shown in Fig. 2(b)) between the tooth surfaces and the intermediate surface S. Nodes and elements are automatically derived from the prescribed number of elements for this mesh and independently of the number of elements defined for the tooth body mesh. Here, linear o quadratic elements can be considered.

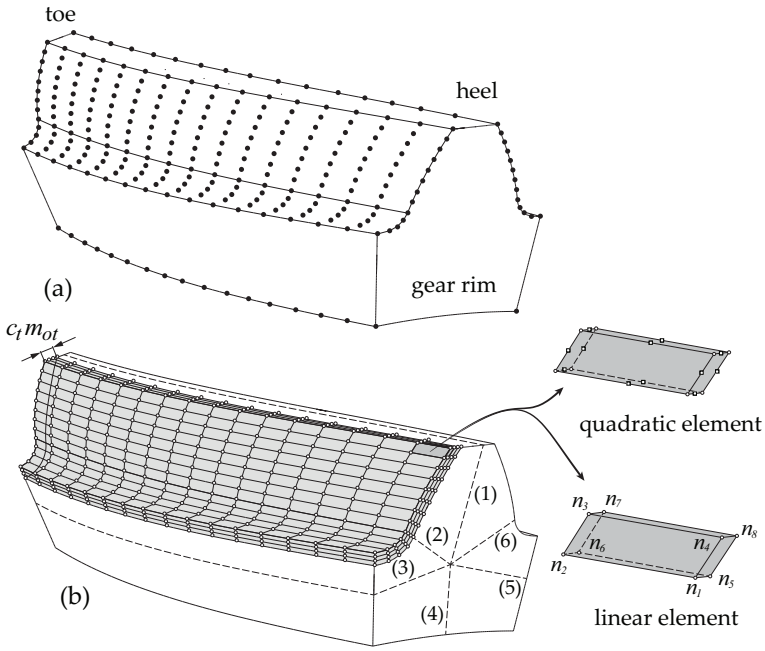

Fig. 2. For mesh definition of contact-fillet region: (a) designed volume with obtained points from application of gear theory, and (b) nodes and finite elements.

(6) A master surface is defined on the tooth body mesh and a slave surface is defined on the contact-fillet region mesh for each gear tooth of the model (see Fig. 3). The master surface is conformed by those nodes of the tooth body mesh that belong to the intermediate surface S. The slave surface is conformed by those nodes that belong to the faces of the elements of the contact-fillet region mesh that are closer to surface S. A tie-surface constraint is defined between the master surface and the slave surface, which means that the nodes of the slave surface are tied to the master surface. Such a constraint allows independency in the definitions of the two described meshes and assures transmission of displacements and loads between the two meshes [19].

(7) Connection between several teeth of the finite element model is accomplished through the definition of new tie-surface constraints. Figure 4 illustrates schematically the arrangement of slave and master surfaces for the connection of several teeth in the finite element model. The scheme is focused, for the purpose of clarity, on a traverse section of the finite element model, although this arrangement is valid along the face width of the gear. Some elements are called *master elements* because they are used to define a master surface. Some other elements are called *slave elements* because they are used to define a slave surface. Some other elements are called *master/slave elements* because one of its faces is used to be part of a master surface and some other face is used to be part of a slave surface. Figure 4 illustrates the connection of three teeth and the same ideas can be applied to connect five or seven teeth. For the example illustrated in Fig 4, slave surfaces s_{11} and s_{12} are tied to master surface m_1, whereas slave surfaces s_{21} and s_{22} are tied to master surface m_2. The arrangement has been established taking into account that a node of a slave surface can be tied to just one master surface and a node of a master surface can be at the same time slave of another master surface [19].

(8) A node-based surface is defined on the inner part and on both sides of the gear rim to conform a rigid surface (see Fig. 4). Boundary conditions of the gear model are applied to this surface. Since the nodes of this surface will have restrictions on their degrees of freedom, they cannot belong to a slave surface but can be part of a master surface [19]. A 3D view of the rigid surface is shown in Fig. 5(a) for a three-tooth model. The rigid surface is rigidly connected to a reference node that is defined on the axis of rotation of the gear. All the degrees of freedom of the reference node govern now the degrees of freedom of the rigid surface. In the case of the pinion, all the degrees of freedom of the reference node are constrained but the rotation around the gear axis is released. A torque around the gear axis of rotation is then applied

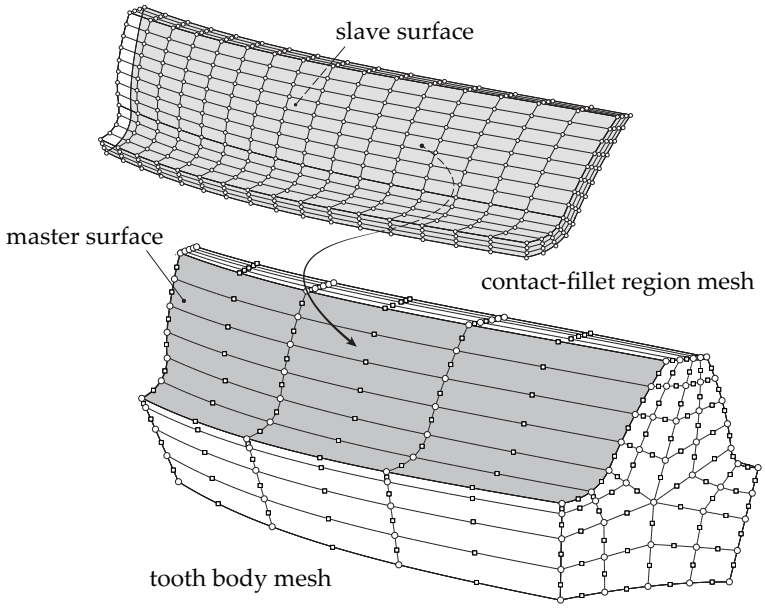

Fig. 3. For illustration of the tie-surface constraint between the nodes of the slave surface and the master surface for one tooth of the gear model.

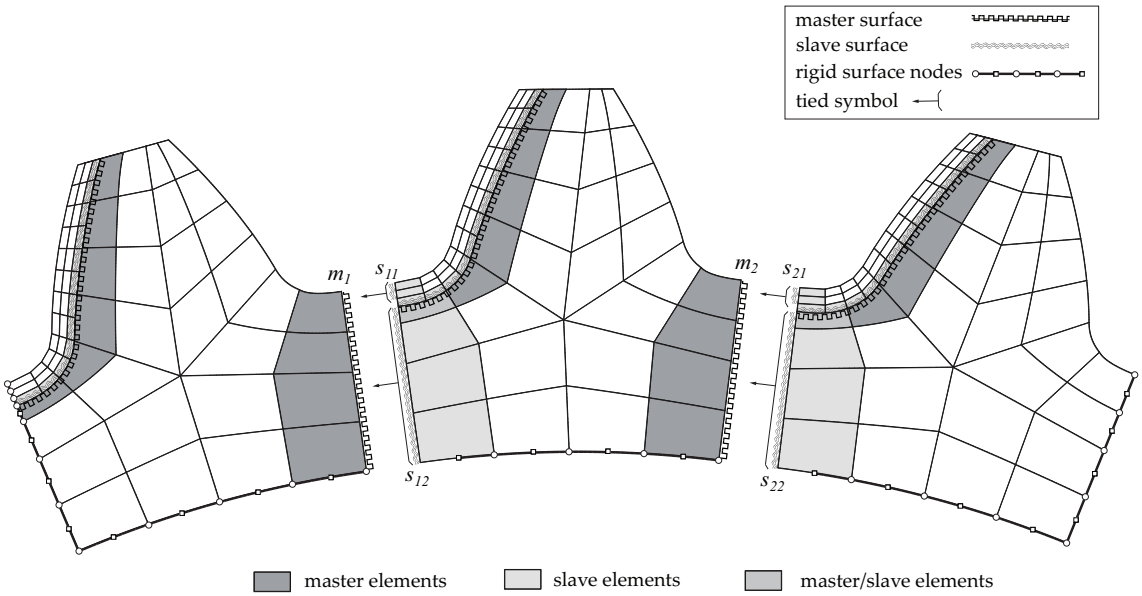

Fig. 4. Scheme in a transverse section at the heel of the gear teeth for illustration of: (i) slave and master surfaces to connect several teeth, and (ii) rigid surface for application of boundary conditions.

to this reference node and therefore to the rigid surface. In the case of the driven gear, the reference node is blocked at each contact position obtained from the application a tooth contact analysis algorithm.

(9) The possibility of a model comprising all the teeth of the gear drive is considered as well. In this case, those teeth that will not come into contact during the analysis of the cycle of meshing are modeled with just six quadratic elements as it is illustrated in Fig. 5(b). The connection between these teeth and the teeth that will come into contact during the analysis of the cycle of meshing is arranged through master-slave surface constraints. The connection between each tooth of this group of teeth that will not come into contact is arranged by using common nodes in the gear rim region. Regarding the rigid surface, it is conformed by those nodes that are in the inner part of the gear rim and do not belong to any slave surface.

(10) The contact formulation between pinion and gear is defined through an algorithm based on the interactions between a master surface and a slave surface [19]. In a model defined with n pairs of contacting teeth, $n = \{1,3,5,7\}$, n master-slave surface interactions are defined. The master surfaces are considered usually at the driven gear since the curvatures of its tooth surfaces are lower than the curvatures of the pinion tooth surfaces.

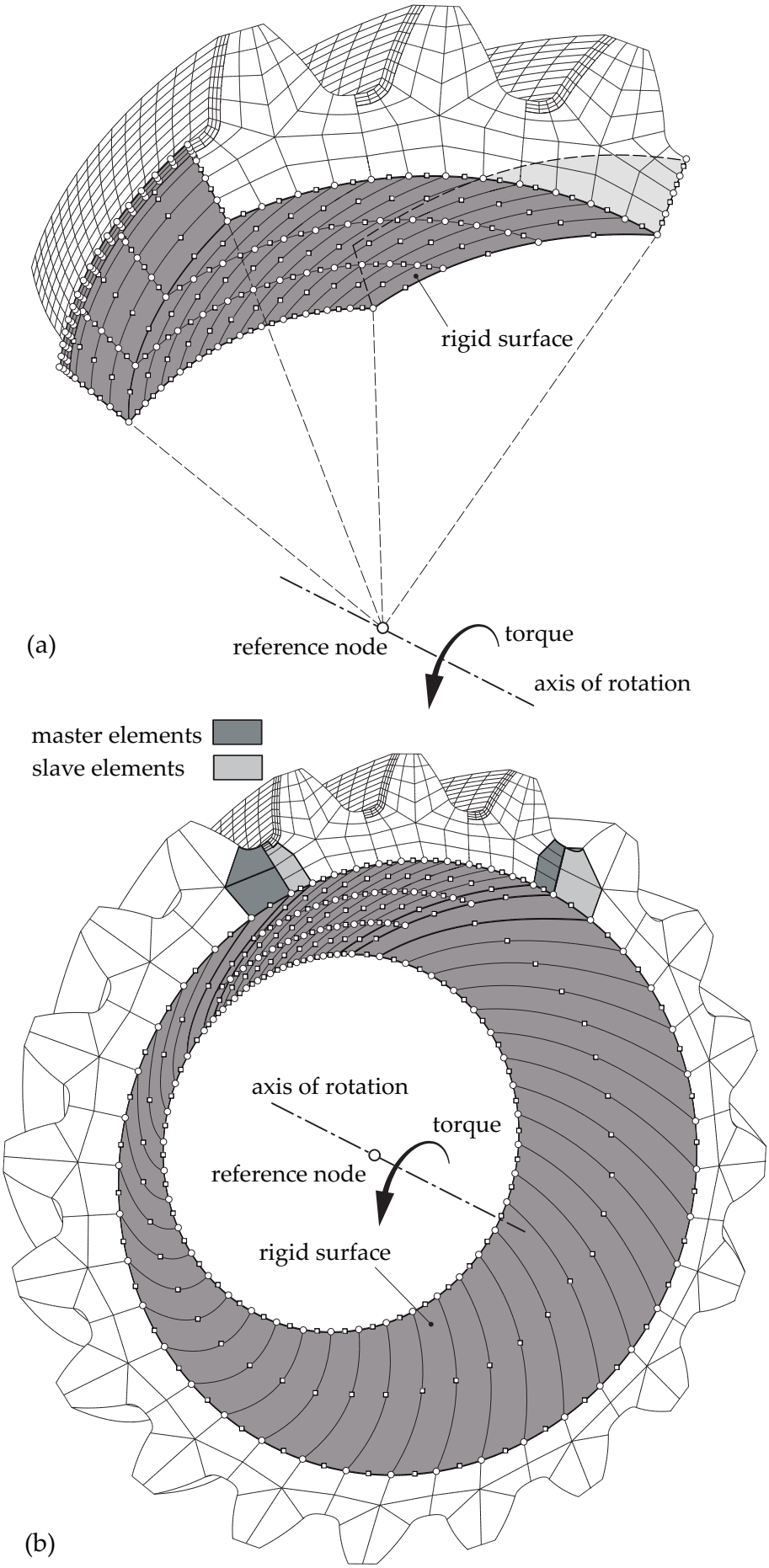

Fig. 5. For illustration of the rigid surface in, (a) a three-tooth finite element model and, (b) a all-tooth finite element model, of the pinion.

3 Numerical examples

A spiral bevel gear drive with localized bearing contact is considered here for the purpose of illustration of the features of the proposed finite element model. The basic data of the transmission is shown in Table 1 whereas the blank data are illustrated in Table 2. A generating face-hobbing process based on the cyclo-palloid© method [20] has been considered here for the localization of the bearing contact. Details of the mathematical model of this method and the involved variables and nomenclature can be found in [21]. Additional cutter data and basic machine-tool settings are shown in Table 3 for three cases of design. Each case of design is provided with a different amount of crowning by considering different values for the cutter radii r_{ci} and r_{co} (see [21]). The third case of design is provided as well with profile crowning by considering parabolic profiles with a parabola coefficient $a_p = 0.0015\,\text{mm}^{-1}$.

Table 1. Basic transmission and cutter data.

Data	Value
Reference gear ratio	1.5
Shaft angle [degrees]	90.0
Input power [KW]	60.0
Pinion speed [rpm]	1500.0
AGMA quality number	8
Cutter radius [mm]	55.0
Number of blade groups	5

Table 2. Blank data.

Blank Data	Pinion	Gear
Tooth number	$N_1 = 20$	$N_2 = 31$
Pitch angle [degrees]	$\gamma_1 = 32.829$	$\gamma_2 = 57.171$
Spiral angle [degrees]	$\psi_m = 35.0$	
Hand of spiral	left-hand	right-hand
Outer transverse module [mm]	$m_{ot} = 4.566$	
Mean normal module [mm]	$m_{mn} = 3.163$	
Mean cone distance [mm]	$A_m = 71.223$	
Face width [mm]	$F_w = 26.0$	
Outer addendum [mm]	$a_{01} = 3.163$	$a_{02} = 3.163$
Outer dedendum [mm]	$b_{01} = 3.795$	$b_{02} = 3.795$
Face cone angle [degrees]	$\gamma_{F1} = 32.829$	$\gamma_{F2} = 57.171$
Root cone angle [degrees]	$\gamma_{R1} = 32.829$	$\gamma_{R2} = 57.171$
Minimum normal backlash [mm]	$B = 0,150$	
Mean normal chordal addendum [mm]	$a_{c1} = 3.230$	$a_{c2} = 3.191$
Mean normal chordal tooth thickness [mm]	$t_{n1} = 4.907$	$t_{n2} = 4.909$

The obtained gear drive and the contact patterns for the three designs are illustrated in Fig. 6. These results are based on the application of a TCA algorithm applied before in [22] and based in [23]. Here, the gear tooth surfaces are assumed

Table 3. Additional cutter data and basic machine-tool settings for three cases of design.

	Case 1		Case 2		Case 3	
Data	Pinion	Gear	Pinion	Gear	Pinion	Gear
Reference radius inner blades, r_{ci} [mm]	55.0	55.0	55.0	55.0	55.0	55.0
Reference radius outer blades, r_{co} [mm]	57.4	57.4	56.4	56.4	55.4	55.4
Parabola coef. inner blades, a_{pi} [mm^{-1}]	0.0	0.0	0.0	0.0	0.0015	0.0
Parabola coef. outer blades, a_{po} [mm^{-1}]	0.0	0.0	0.0	0.0	0.0015	0.0
Slope angle, ν [degrees]	8.017	8.001	8.170	8.154	8.327	8.311
Inner machine distance, M_{di} [mm]	67.400	67.386	67.538	67.524	67.680	67.666
Inner cradle angle, q_{2i} [degrees]	46.652	46.656	46.609	46.614	46.566	46.570
Outer machine distance, M_{do} [mm]	67.930	67.917	67.837	67.823	67.763	67.748
Outer cradle angle, q_{2o} [degrees]	48.653	48.658	47.779	47.784	46.901	46.905
Machine center to back, ΔX_D [mm]	0.0	0.0	0.0	0.0	0.0	0.0
Blank offset, ΔE_m [mm]	0.0	0.0	0.0	0.0	0.0	0.0
Sliding base, ΔX_B [mm]	0.0	0.0	0.0	0.0	0.0	0.0
Machine root angle, γ_m [degrees]	32.829	57.171	32.829	57.171	32.829	57.171
Gear-to-cradle roll ratio, m_{gc}	1.844587	1.190056	1.844587	1.190056	1.844587	1.190056
Gear-to-blade roll ratio, m_{gb}	0.242516	0.156160	0.247119	0.159126	0.251850	0.162174

to behave as rigid surfaces. A marking compound thickness of 0.0065 mm is considered to determine the size of the contact ellipses. The algorithm is based on minimization of the distances between the rigid surfaces and works properly for line, point or edge contacts.

In order to validate the proposed finite element model, the following subsections are considered:

(i) Application of the Hertz's theory.
(ii) Validation of the proposed finite element model by comparing contact stresses and Hertz stresses.
(iii) Observation of convergency for bending stresses.
(iv) Investigation of contact and bending stresses along the cycle of meshing.
(v) Investigation of transmission errors along the cycle of meshing.

3.1 Application of the Hertz's theory

In order to validate the proposed finite element model in terms of contact behaviour, the Hertz's theory was applied to the three cases of design. The same ideas that were developed in [17] for implementation of the Hertz's theory in a spur gear drive with double crowned tooth surfaces, are considered here. For the Hertz's hypothesis [15] to be satisfied, the bearing contact needs to be localized inside the tooth surfaces and to be elliptical, as it occurs for the three cases of design shown in Fig. 6.

The implemented algorithm for Hertz's analysis is similar to the one implemented in [17] for a single point of contact. A mean contact position is chosen along the cycle of meshing. The whole load is considered to be shared between just one pair of contacting teeth. This makes easier the application of the Hertz's theory to a gear drive and is enough to test locally the contact behaviour of the proposed finite element model. The sharing of the load between several pairs of teeth is considered later, from Subsection 3.3 on.

The results provided by the implemented algorithm to the three cases of design are illustrated in Table 4. The chosen contact position is the number 12 of a total of 21 contact positions. Principal curvatures are computed numerically from an interpolated surface that is built upon a grid of 41×41 points that belong to a reference surface. This reference surface represents the gap between pinion and gear tooth surfaces at the chosen contact position (more details about the applied algorithm can be view in [17]). Complete and incomplete elliptical integrals of first kind and second kind [15] have been computed numerically by Simpson 1/3 rule [24]. The gear materials are steel with elastic modules $E_1 = E_2 = 210000$ MPa and Poisson's coefficients $\nu_1 = \nu_2 = 0.3$. The considered applied torque is 380.0 Nm (see Table 1).

The evolutions of principal stresses and effective Mises and Tresca stresses underneath the contacting surfaces at the mean contact position 12 are illustrated in Fig. 7 for case 2 of design. The depth of maximum Mises stresses occurs at $0.71b$

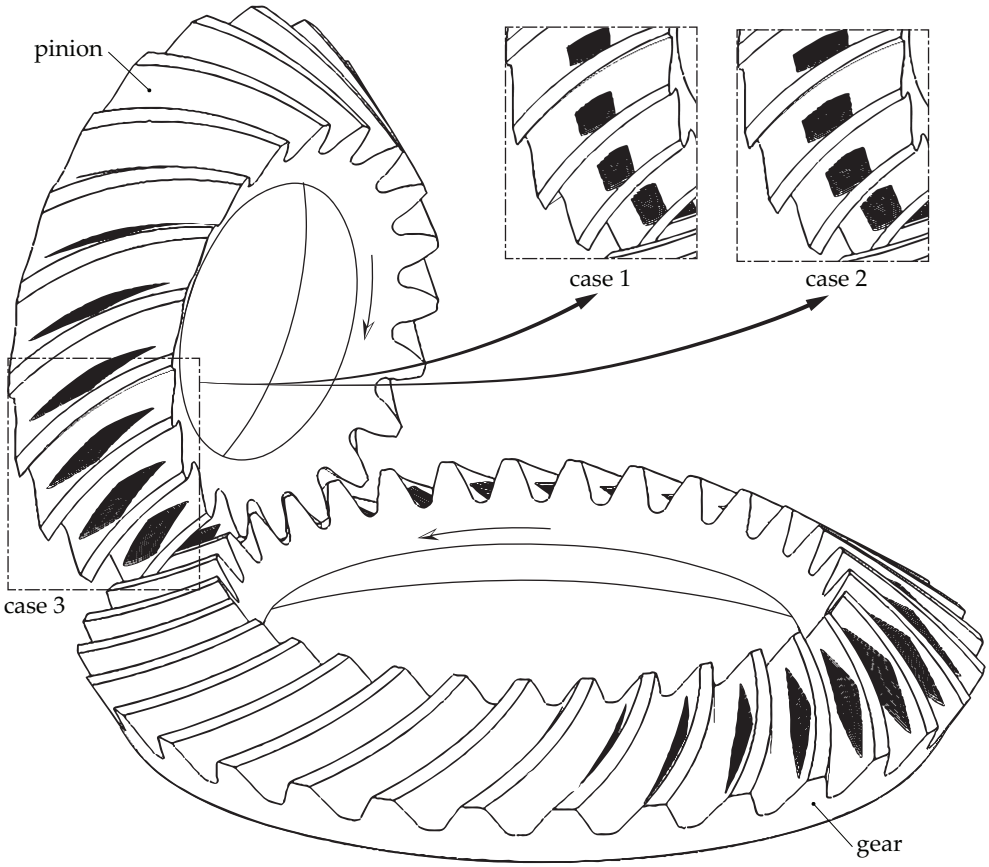

Fig. 6. Gear drive model and contact patterns corresponding to three cases of design.

whereas the depth of maximum Tresca stress occurs at $0.78b$.

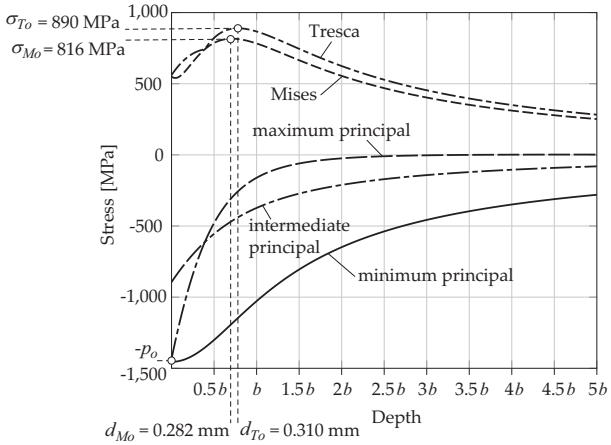

Fig. 7. Evolution of stresses underneath the contacting surfaces for case 2 of design at mean contact position 12 obtained from application of Hertz's theory.

3.2 Validation of the proposed finite element model by comparing contact stresses and Hertz stresses

A number of finite element models with just one pair of contacting teeth are built following the procedure described in Section 2 for case of design 2 (see Fig. 8(a)). A coefficient $c_t = 0.2$ (see Fig. 1(b)) and three layers of quadratic elements in the contact-fillet region (see Fig. 2) are considered for these models. The models are built considering different number of elements in profile (n_p) and longitudinal (n_l) directions. Figure 8(b) shows that convergency of the results occur for contact area A_c, maximum contact pressure p_o, maximum Mises stress σ_{M_o}, and maximum Tresca stress σ_{T_o} as the number n_p of

Table 4. Results from application of the algorithm based on the Hertz's theory.

Result	Case 1	Case 2	Case 3
Major principal curvature radius, R_I [mm]	1623.5	2779.7	3731.2
Minor principal curvature radius, R_{II} [mm]	15.8	15.8	15.4
Equivalent applied force at the contact position, F [N]	12781.9	12781.9	12735.3
Equivalent elastic modulus, E^* [MPa]		115384.6	
Major semi-length of contact ellipse, a [mm]	8.610	10.570	11.813
Minor semi-length of contact ellipse, b [mm]	0.439	0.397	0.370
Contact area, A_c [mm^2]	11.876	13.179	13.737
Maximum contact pressure, p_o [MPa]	1614.4	1454.7	1390.6
Maximum Mises stress, σ_{M_o} [MPa]	908.0	816.4	779.6
Maximum Tresca stress, σ_{T_o} [MPa]	991.6	889.7	848.6
Depth maximum Mises stress, d_{M_o} [mm]	0.312	0.282	0.263
Depth maximum Tresca stress, d_{T_o} [mm]	0.342	0.310	0.289

elements is increased (all these models have 64 elements in longitudinal direction and 16 elements in the fillet direction and are named as models $64 \times n_p \times 16$). The same observation can be done when the number n_l is increased (see Fig. 8(c) for models with 48 elements in profile direction and 16 elements in the fillet direction, which are named as models $n_l \times 48 \times 16$). It is observed that increasing the number n_p has a larger influence in the convergency of the results than increasing the number n_l. It is observed as well that the model $64 \times 48 \times 16$ provide similar results to the ones obtained by using models with a finer mesh.

Models $64 \times 48 \times 16$ are built considering different values of coefficient c_t and either linear or quadratic elements. Figure 9 shows the contact pressure distribution on the pinion tooth surface for case 2 of design with $c_t = 0.2$ and $c_t = 0.125$. Here, 3 layers of quadratic elements are considered in the contact-fillet region mesh. Evolution of maximum contact pressure and contact area is illustrated in Figure 10 considering several values of coefficient c_t. It is observed that a very thin layer in the contact-fillet region mesh is accompanied by high values of contact pressures. However, an increment in the coefficient c_t leads to an approximation of the results to the Hertz results. Similar conclusions can be observed as well for cases 1 and 3 of design. A thickness of the contact-fillet region about $c_t = 2b/m_{ot}$ or $c_t = 2.5b/m_{ot}$ is favorable to get maximum contact pressures with relative errors below the 5% respect to the maximum contact pressure obtained in the Hertz analysis. If the contact-fillet region is very thin and the intermediate surface S (see Fig. 1) is very close to the contacting surface, the deformation of the contact-fillet region mesh leads to an uneven distribution of contact pressure as it is shown in Fig. 9(b).

The proposed model can capture the maximum value of Mises or Tresca stress underneath the contacting surfaces. Figure 11(a) shows in detail the maximum Mises stress for case 2 of design when 3 layers of quadratic elements are considered. A cut section in the contact-fillet region mesh allows the stress distribution to be visualized inside the contact model. Figures 11(b) and (c) shows the variation of Mises and Tresca stresses when different coefficients c_t and types of elements (linear o quadratic) are considered. The represented stresses are extrapolated values at the nodes with an average threshold of 75% [19]. The results show that maximum Mises and Tresca stresses approach the Hertz result as coefficient c_t is increased. However, the results are not so close to the Hertz results as the maximum contact pressures are.

3.3 Observation of convergency for bending stresses

Bending stresses are evaluated considering the major principal stress σ_1 in the fillet of the middle tooth. Validation of the finite element model for bending stresses is executed through observation of convergency of the results at a given contact position. Figure 12 shows that, indeed, convergency occurs either for linear elements or quadratic elements when the number of elements in the fillet direction n_f is increased. Case 2 of design is considered here at contact position number 12. A three-tooth model allows the boundary conditions of the rigid surface to be far enough from the fillet area where stresses are obtained. Three types of elements in the contact-fillet region are considered (see [19]): (i) C3D8 elements (linear elements with eight nodes), (ii) C3D20 elements (quadratic elements with 20 nodes), and (iii) C3D8I (linear elements with 8 nodes and incompatible modes of deformation to improve its bending behaviour). A difference about 40 MPa is observed between elements C3D8 and C3D20 when $n_f = 20$, which represents approximately a 10% of relative error. However,

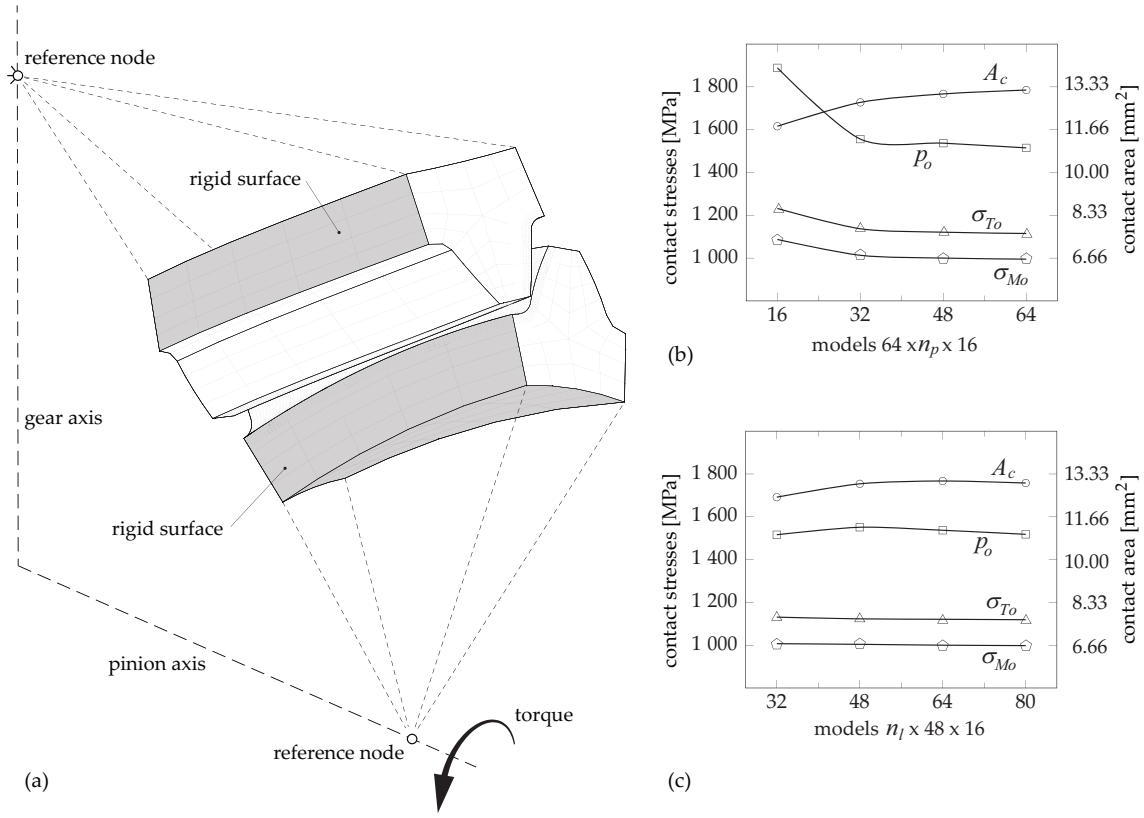

Fig. 8. Finite element model (a) for investigation of convergency of contact stresses and contact area for case 2 of design when varying the number of profile elements n_p (b) and the number of longitudinal elements n_l (c).

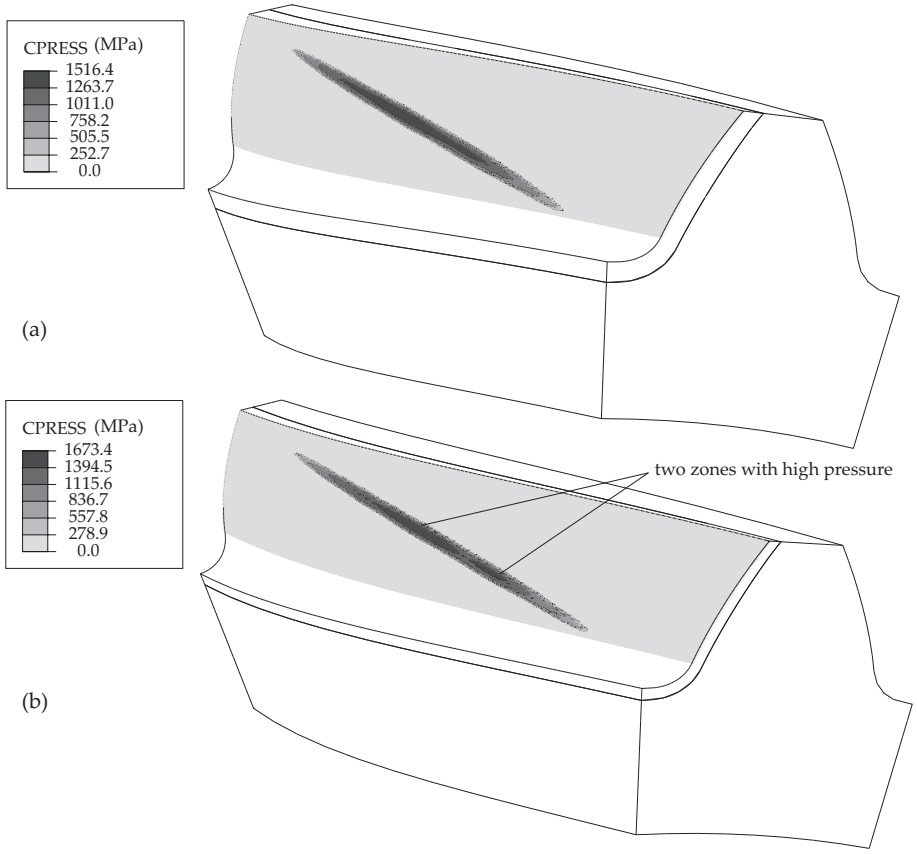

Fig. 9. Contact pressure distribution in case 2 of design for (a) $c_t = 0.2$ and (b) $c_t = 0.125$ with three layers of quadratic elements.

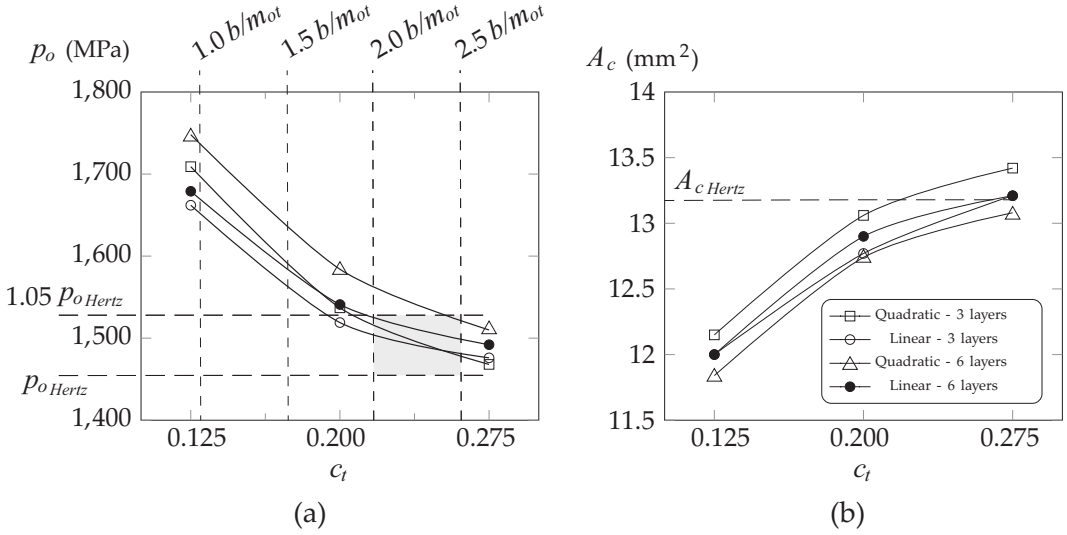

Fig. 10. Variation of maximum contact pressure (a) and contact area (b) in case 2 of design considering models $64 \times 48 \times 16$ with different coefficients c_t, linear or quadratic elements, and three or six layers of elements.

comparing elements C3D8I with elements C3D20, the relative error is reduced below 0.5% when $n_f = 20$. Some more models considering elements C3D8I with $n_f = 24$ and $n_f = 28$ are analyzed to prove that convergency occurs as well for this type of element.

3.4 Investigation of contact and bending stresses along the cycle of meshing

Case 3 of design is considered for investigation of contact and bending stresses along the cycle of meshing. This design is provided with an adjusted contact pattern in diagonal direction (see Fig. 6) and a parabolic function of unloaded transmission errors (see below). Two cycles of meshing are analyzed through 21 contact positions by considering a tooth contact analysis algorithm where three pairs of contacting teeth are taken into account. Since maximum contact stresses (contact pressure, Mises stress and Tresca stress) are obtained in the contact region mesh of the whole model, periodicity of the evolution of these variables along the two cycles of meshing is expected. Maximum major principal stress for evaluation of the bending behaviour of the gear drive is measured at the fillet region mesh of the middle tooth for each model along the 21 contact positions.

The finite element models are built with a mesh $64 \times 48 \times 16$ considering either linear elements (C3D8 and C3D8I) or quadratic elements (C3D20) for the contact-fillet region mesh, and quadratic elements (C3D20) for the body region mesh. Models with three pairs of teeth, five pairs, and seven pairs, are built. Their corresponding counterparts considering the same number of contacting teeth and all the other teeth of the gear drive are built as well (these models are identified with the adjective complete). The models are built with a coefficient $c_t = 0.25$ and three layers of elements in the contact-fillet region. Figure 13 shows the finite element model and its corresponding counterpart when five pairs of contacting teeth are considered. The rigid surfaces are defined for each type of model and for each gear member as it is illustrated in Fig. 5 for the pinion member.

Figures 14(a) and (b) show the evolutions of maximum contact pressure p_o and maximum major principal stress σ_{1_o}, respectively, along two cycles of meshing and considering the three types of elements, mentioned above, for the contact-fillet region mesh. A three tooth pair model is considered here for the purpose of comparison of the results that the three types of elements provide. Results of p_o are obtained, in this example, just at the middle pair of contacting teeth (pair 0). Contact and bending stresses are illustrated in Fig. 14(c) in a three teeth pinion model for contact position 18. Figure 14(a) shows that the three types of elements provide similar values of p_o from contact position 1 to contact position 15. However, it is observed larger values of p_o for the model with elements C3D20 from contact position 16 to contact position 21 (see shaded area). In this part of the cycle of meshing, a truncation of the contact ellipse occurs and edge contact appears at the middle tooth pair (as it can be visualized in Fig. 14(c)). Although it is expected an increment of contact stresses for this circumstance, local deformations may lead to a determined increment of the stresses. This increment may not be accurately determined with an approach that is just based on an elastic behaviour of the materials as the one that this work is based on. However, it can be drawn that elements C3D20 provide much higher values of p_o when edge contact occurs than elements C3D8 or C3D8I.

Regarding bending stresses and taking as a reference the results provided by a model with elements C3D20, Figure 14(b) shows that a model with elements C3D8I provides closer values of σ_{1_o} than the ones provided by a model with elements C3D8. In this case, the maximum relative error for a model with elements C3D8I is $\varepsilon_{max} = 3.2\%$ whereas for a model with elements C3D8 is $\varepsilon_{max} = 10.2\%$.

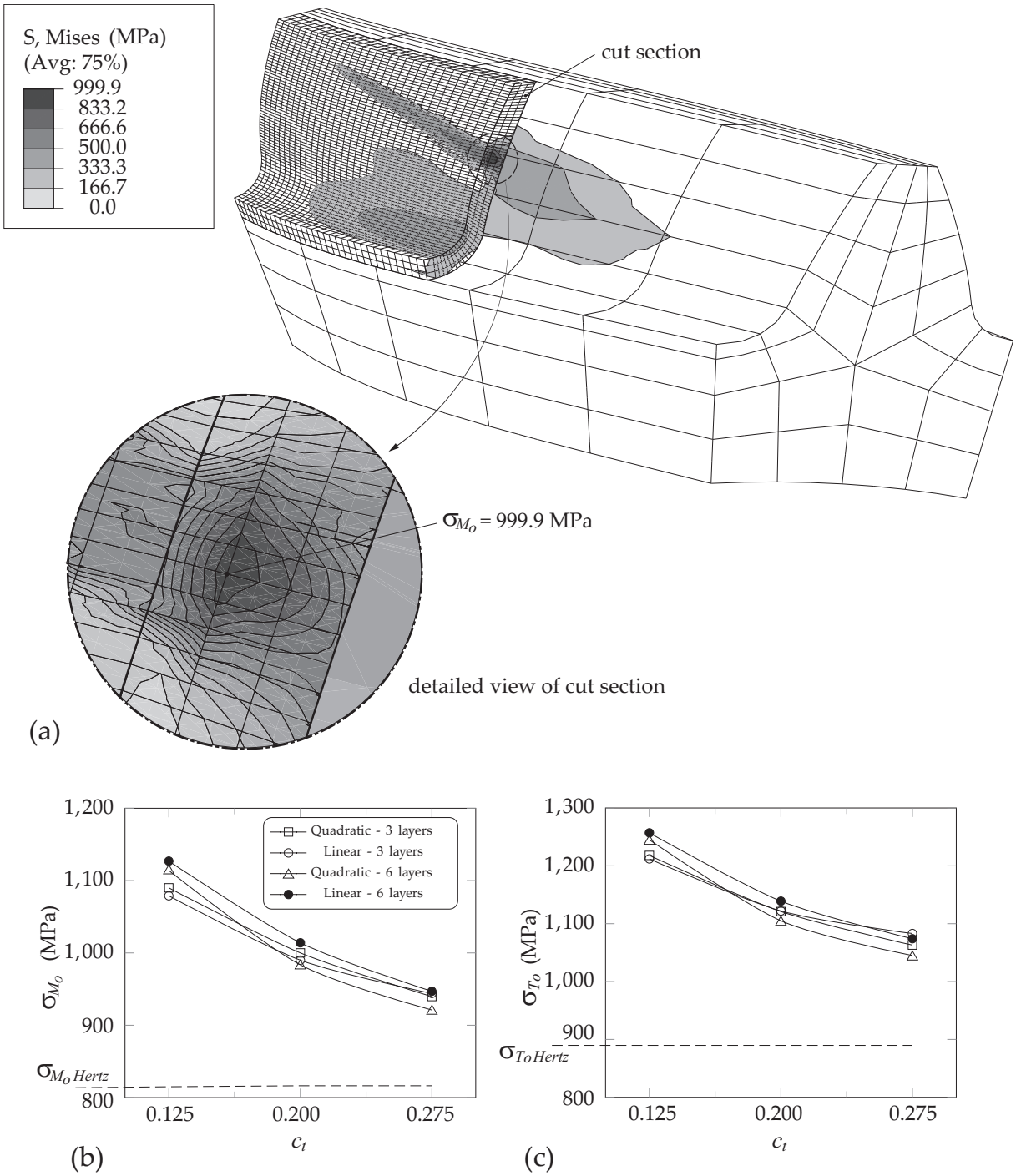

Fig. 11. Mises and Tresca stresses for several analysis of case 2 of design considering models $64 \times 48 \times 16$: (a) Mises distribution for $c_t = 0.2$ and 3 layers of quadratic elements, (b) maximum Mises, and (c) maximum Tresca for several values of coefficient c_t, type of element and number of layers.

Figure 15 shows the evolution of p_o along two cycles of meshing, evaluated at each contact pair, for models with three and five pairs of contacting teeth and for its corresponding complete models. Linear elements C3D8I are used here for the contact-fillet region mesh whereas elements C3D20 are used for the body region mesh. The area below the curve that describes the evolution of maximum p_o is shaded in order to highlight its grade of periodicity. For this purpose, the maximum values of p_o at contact positions 1, 11, and 21, are outlined as well. Pairs of contacting teeth are enumerated according to Fig. 13(a). It is observed an improvement of the periodicity in the evolution of p_o as the number of pairs of contacting teeth is increased from three to five (compare Figs. 15(a) and (c)), since pairs +2 and -2 come into contact when five pairs of contacting teeth are considered. An improvement of the periodicity is also observed for a complete model in comparison with its corresponding counterpart (compare Figs. 15(a) and (b) or Figs. 15(c) and (d)). The boundary conditions imposed

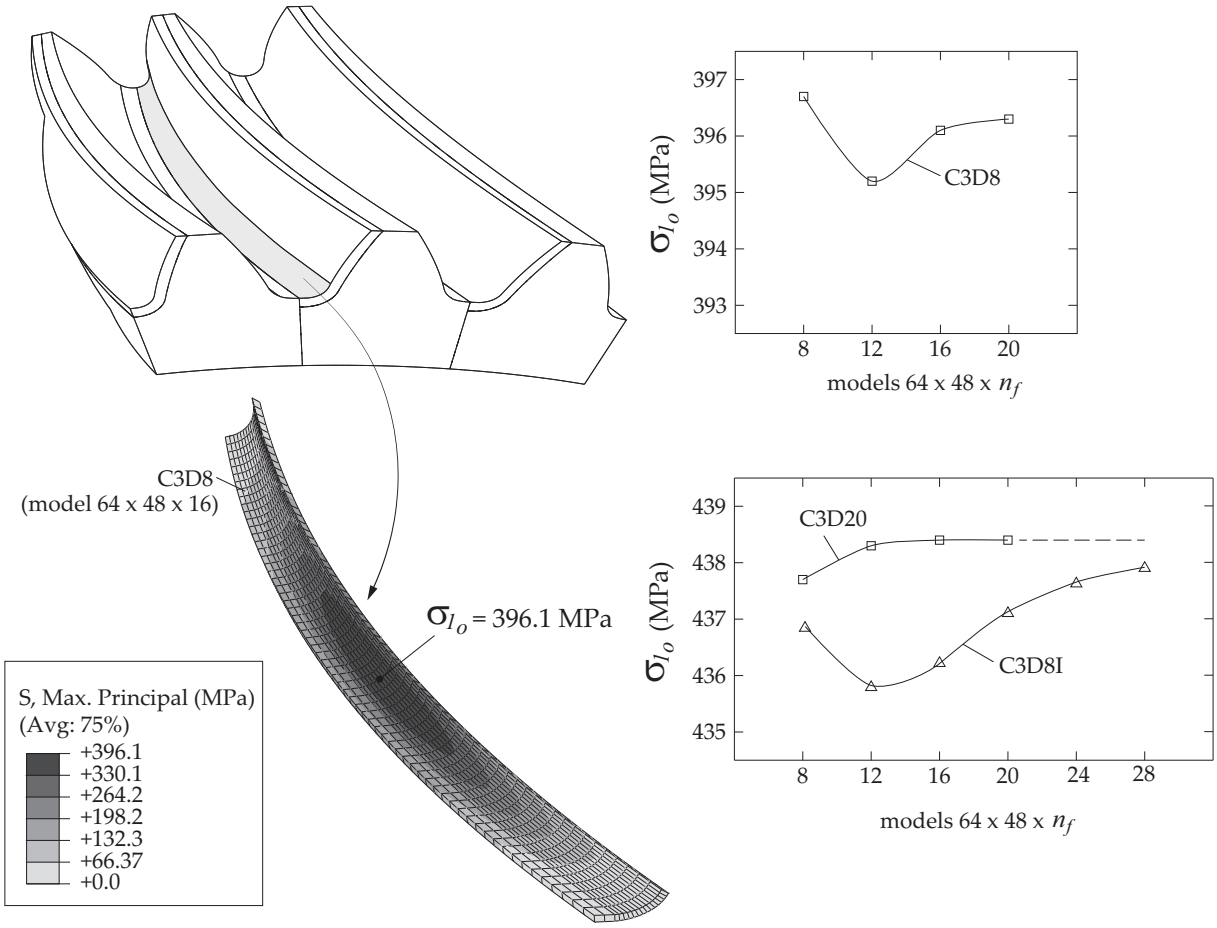

Fig. 12. For illustration of convergency of maximum major principal stress σ_{1o} in the fillet region of the middle tooth for several values of the number of elements in the fillet direction n_f and different types of elements.

by the rigid surface in a complete model (see Fig. 5(b)) provide an improvement of the periodicity of p_o evolution respect to the boundary conditions imposed by the rigid surface in a non-complete model (see Fig. 5(a)). However, this improvement is not so important as the improvement when increasing the number of contacting teeth. The results that are obtained in models with seven pairs of contacting teeth are very similar to those obtained through application of models with five pairs of contacting teeth, and are not illustrated here.

Regarding bending stresses, since maximum major principal stress σ_{1_o} is measured at the middle tooth of the gear model, no important differences are observed between considering a three tooth pair model, a five tooth pair model, or a seven tooth pair model.

3.5 Investigation of transmission errors along the cycle of meshing

Case 3 of design is provided with a parabolic function of transmission errors. This function can be obtained from application of a TCA algorithm (see [21]) and is called function of unloaded transmission errors, since no load is still applied. A function of loaded transmission errors can be then obtained through the determination of the rotational angle of the pinion reference node, at each contact position, when a torque is applied to the pinion model. Such a rotational angle counts for the elastic deformations of the gear tooth surfaces when the load is applied. The function of total transmission errors is then obtained as a sum of both previous mentioned functions. Details of derivation of the function of loaded transmission errors and total transmission errors can be found in [8] with a different finite element model.

Figure 16 shows the functions of unloaded, loaded, and total transmission errors, for the proposed models with three, five, and seven pairs of contacting teeth, and their corresponding counterpart complete models. Elements C3D8I at the contact-fillet region mesh and elements C3D20 at the body region mesh are considered here. The function of unloaded transmission errors is the same in all the graphs illustrated in Fig. 16 since the same case of design is considered. The area below the function of total transmission errors is shaded to highlight the periodicity of this function. For this purpose, the maximum and minimum values of the function of total transmission errors are outlined as well through dashed lines. Is is observed an improvement of the periodicity of the function of total transmission errors as the number of contacting teeth is

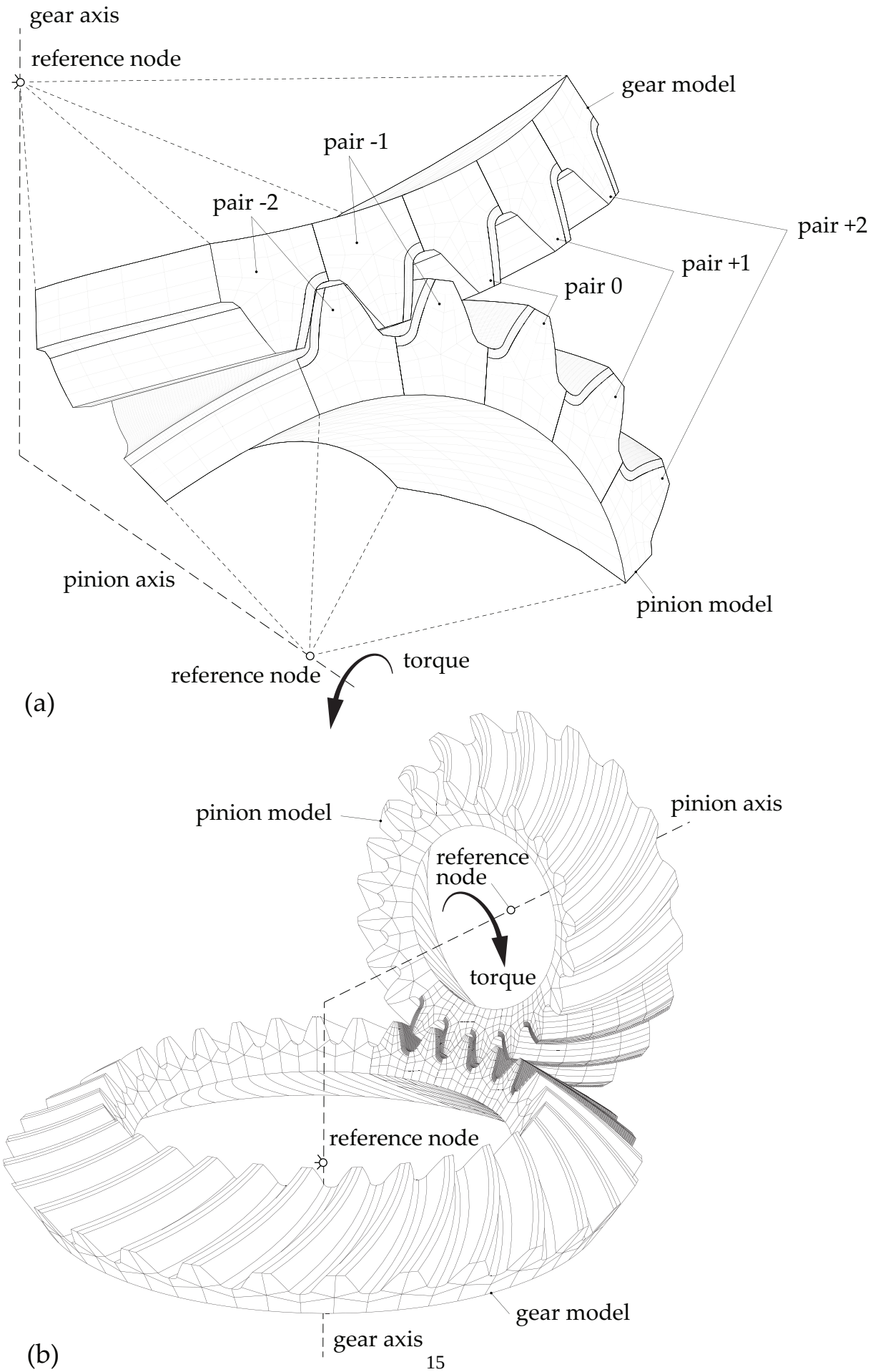

Fig. 13. Finite element models based on (a) five pairs of contacting teeth (5 tooth pair model) and (b) five pairs of contacting teeth and all the other teeth of the gear drive (5 tooth pair complete model).

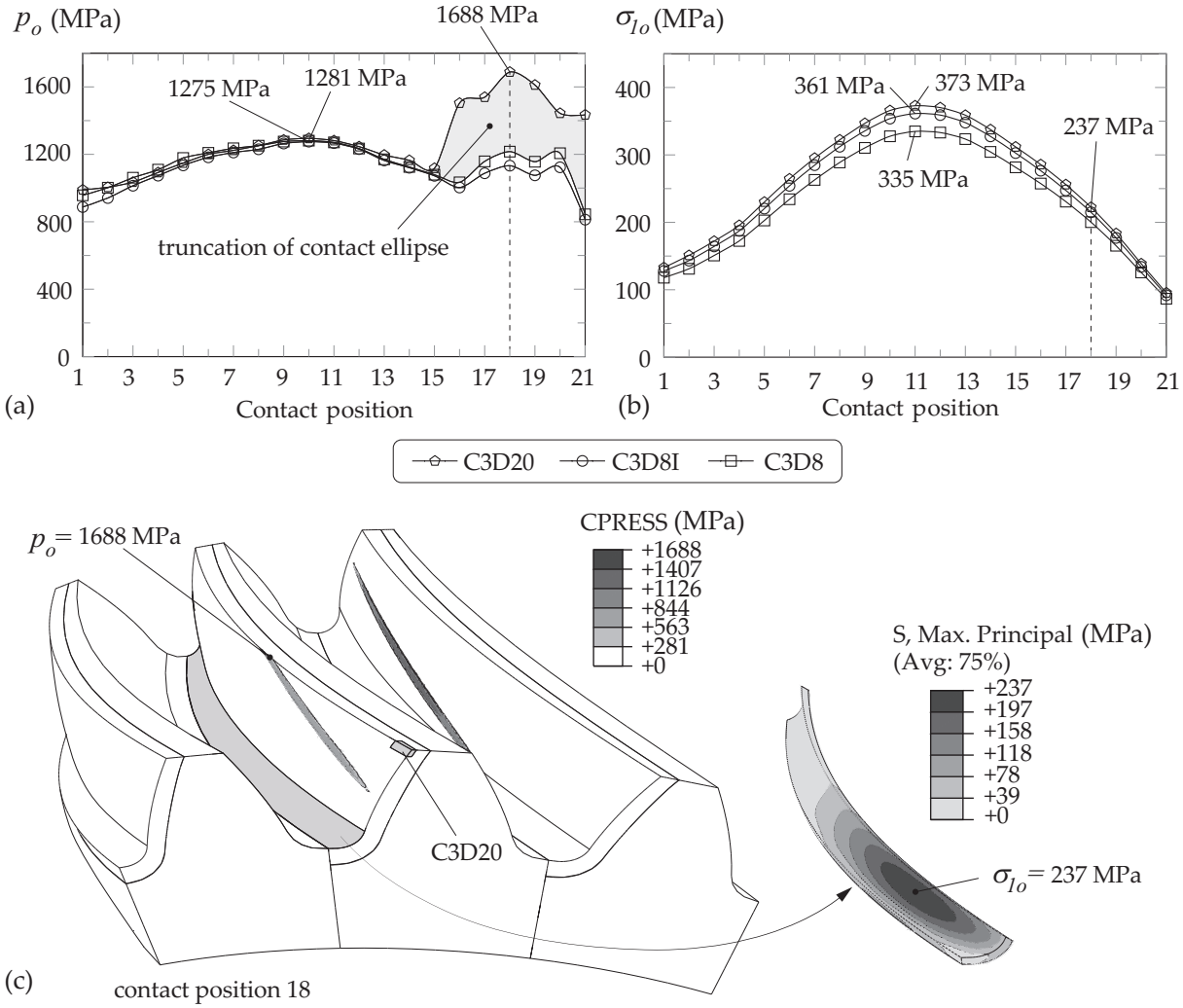

Fig. 14. Maximum contact pressures p_o and maximum major principal stresses σ_{1_o} along two cycles of meshing at the middle tooth of a 3 tooth pair model for illustration of different behaviour of element types C3D20, C3D8I, and C3D8.

increased from three to seven (compare Figs. 16(a), (c), and (e)). It is observed as well that the periodicity of the function of total transmission errors obtained in a complete model is better respect to the one obtained in its corresponding counterpart model (compare Figs. 16(a) and (b) for three pairs of contacting teeth, or Figs. 16(c) and (d) for five pairs of contacting teeth). However, no differences in the periodicity of the function of total transmission errors between a complete model and its corresponding counterpart model are observed when seven pairs of contacting teeth are considered (compare Figs. 16(e) and (f)).

4 Conclusions

Based on the performed research and results obtained, the following conclusions can be drawn:

(1) A new finite element model based on the application of tie-surface constraints is proposed and validated in terms of contact and bending stresses.
(2) The proposed model is able to capture the maximum value of effective Mises stress and effective Tresca stress underneath the contacting surfaces. However, these values are overestimated respect to the values obtained from application of the Hertz's theory.
(3) Maximum contact pressure values are in good agreement with the values obtained from the Hertz's theory. Some recommendations are given to establish the thickness of the contact-fillet region in the proposed finite element model.
(4) Quadratic and linear elements are compared in terms of maximum contact pressure and maximum major principal stress for evaluation of contact and bending stresses. Both types of elements provide similar maximum contact pressure values, although quadratic elements show much higher values when edge contact occurs. Linear elements with improved bending behavior show small relative errors of maximum major principal stress, at the fillet, when compared to quadratic

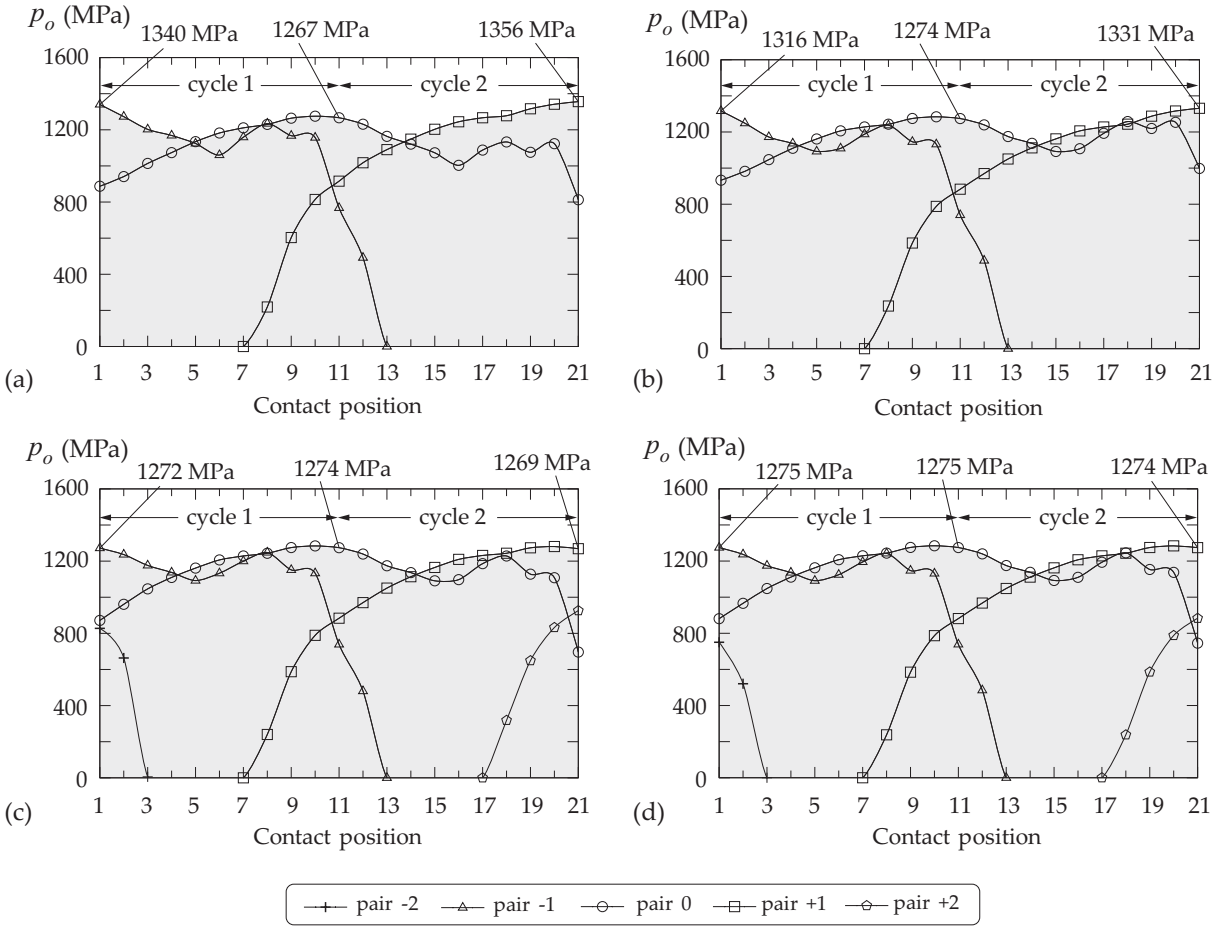

Fig. 15. Maximum contact pressure p_o along two cycles of meshing in a: (a) 3 tooth pair model, (b) 3 tooth pair complete model, (c) 5 tooth pair model, and (d) 5 tooth pair complete model.

elements.

(5) The effect of the rigid surfaces on the evolution of maximum contact pressure, maximum major principal stress, and total transmission errors, is investigated for models with three, five, and seven tooth pairs, and their corresponding counterpart models where all the teeth of the gear drive are considered. The results show that a three tooth pair model is enough for evaluation of the maximum major principal stress, in the fillet of the middle tooth, along the cycle of meshing. The results show as well that the boundary conditions provided by the rigid surface in a five and a seven tooth pair model are far enough from the contact areas to provide, respectively, good periodicity of maximum contact pressure and total transmission errors, making unnecessary the use of compete models as long as other effects as web thickness or web location are not investigated.

Acknowledgments

The authors express their deep gratitude to the Spanish Ministry of Education, Culture, and Sport, for the financial support received through the scholarship Ref. PRX16/00416 from the Program of Mobility Stays for Senior Professors and Researchers at Foreign Centers for High Level Education and Research, in the frame of the Spanish State Program for Scientific and Technical Research and Innovation 2013-2016.

References

[1] L. Wilcox, W. Coleman, Application of finite elements to the analysis of gear tooth stresses, Journal of Engineering for Industry 95 (4) (1973) 1139.

[2] R. F. Handschuh, F. L. Litvin, A method for determining spiral-bevel gear tooth geometry for finite element analysis, NASA Technical Paper 3096, AVSCOM Technical Report 91-C-020 (1991) 1–20.

[3] J. H. Argyris, A. Fuentes, F. L. Litvin,Computerized integrated approach for design and stress analysis of spiral bevel gears, Computer Methods in Applied Mechanics and Engineering 191 (11-12) (2002) 1057–1095.

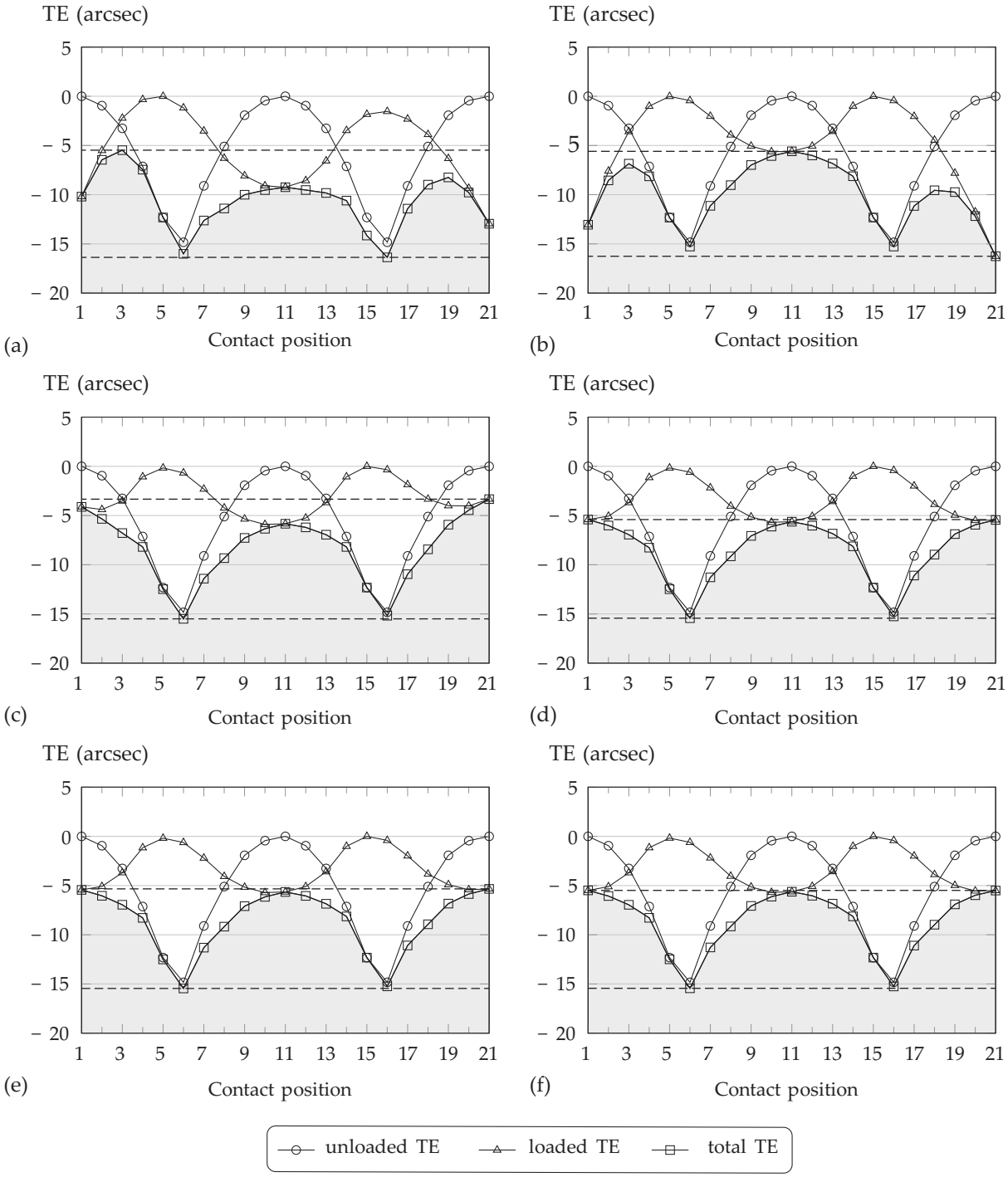

Fig. 16. For illustration of the periodicity grade of the function of total transmission errors (TE) in a: (a) 3 tooth pair model, (b) 3 tooth pair complete model, (c) 5 tooth pair model, (d) 5 tooth pair complete model, (e) 7 tooth pair model, and (f) 7 tooth pair complete model.

[4] I. Gonzalez-Perez, V. Roda-Casanova, A. Fuentes, F. T. Sanchez-Marin, J. L. Iserte,A finite element model for consideration of the torsional effect on the bearing contact of gear drives, Journal of Mechanical Design, Transactions of the ASME 134 (071007) (2012) 1–8.

[5] S. Li, Gear contact model and loaded tooth contact analysis of a three-dimensional, thin-rimmed gear, Journal of Mechanical Design 124 (3) (2002) 511.

[6] I. Gonzalez-Perez, A. Fuentes, V. Roda-Casanova, F. T. Sanchez-Marin, J. L. Iserte, A finite element model for stress analysis of lightweight spur gear drives based on thin-webbed and thin-rimmed gears, International Conference on Gears, VDI-Society for Product and Process Design, 2013, pp. 75–86.

[7] V. Roda-Casanova, F. T. Sanchez-Marin, I. Gonzalez-Perez, J. L. Iserte, A. Fuentes, Determination of the ISO face

load factor in spur gear drives by the finite element modeling of gears and shafts, Mechanism and Machine Theory 65 (2013) 1–13.
[8] A. Fuentes, R. Ruiz-Orzaez, I. Gonzalez-Perez, Compensation of errors of alignment caused by shaft deflections in spiral bevel gear drives, Vol. 34, 2016.
[9] S. M. Vijayakar, Finite element methods for quasi-prismatic bodies with application to gears, Ph.D. thesis, The Ohio State University (1987).
[10] I. Gonzalez-Perez, A. Fuentes, Implementation of a finite element model for stress analysis of gear drives based on multi-point constraints, Mechanism and Machine Theory 117 (2017) 35–47.
[11] K. Mao, Gear tooth contact analysis and its application in the reduction of fatigue wear, Wear 262 (11–12) (2007) 1281–1288.
[12] S. M. Vijayakar, A combined surface integral and finite element solution for a threedimensional contact problem, International Journal for Numerical Methods in Engineering 31 (1991) 525–545.
[13] M. Faggioni, F. S. Samani, G. Bertachi, F. Pellicano, Dynamic optimization of spur gears, Mechanism and Machine Theory 46 (4) (2011) 544–557. 1057–1095.
[14] J. Wang, W. Shen, Z. Wang, M. Yao, X. Zeng, Multi-objective optimization of drive gears for power split device using surrogate models, Journal of Mechanical Science and Technology 28 (6) (2014) 2205–2214. 1057–1095.
[15] K. L. Johnson, Contact mechanics, Cambridge University Press, 1985.
[16] J. J. Coy, C. H. Chao, A method of selecting grid size to account for Hertz deformation in finite element analysis of spur gears, Nasa Technical Memorandum 86263, AVRADCOM Technical Report 81-C-14 (1981) 1–26.
[17] I. Gonzalez-Perez, J. L. Iserte, A. Fuentes,Implementation of Hertz theory and validation of a finite element model for stress analysis of gear drives with localized bearing contact, Mechanism and Machine Theory 46 (6) (2011) 765–783.
[18] F. L. Litvin, A. Fuentes, Gear geometry and applied theory, Cambridge University Press, 2004.
[19] Dassault Systemes, Inc., 2015, *ABAQUS/Standard analysis user's guide*, 175 Wyman Street, Waltham, Massachusetts, United States.
[20] W. Krumme, Klingelnberg-Spiralkegelräder: berechnung, herstellung und einbau, Springer-Verlag, Berlin and Heidelberg, 2013.
[21] I. Gonzalez-Perez, A. Fuentes-Aznar, Analytical determination of basic machine-tool settings for generation of spiral bevel gears and compensation of errors of alignment in the cyclo-palloid system, International Journal of Mechanical Sciences 120 (2017) 91–104.
[22] A. Fuentes, R. Ruiz-Orzaez, I. Gonzalez-Perez, Computerized design, simulation of meshing, and finite element analysis of two types of geometry of curvilinear cylindrical gears, Computer Methods in Applied Mechanics and Engineering 272 (2014), 321–339.
[23] G. I. Sheveleva, A. E. Volkov, V. I. Medvedev, Algorithms for analysis of meshing and contact of spiral bevel gears, Mechanism and Machine Theory 42 (2) (2007) 198–215.
[24] Y. Jaluria, Computer methods for engineering, Taylor & Francis, 1996.

List of Tables

List of Figures